Astron. Astrophys. 342, 809–822 (1999)

ASTRONOMY
AND
ASTROPHYSICS

A 330–360 GHz spectral survey of G34.3+0.15

III. The outer halo

M.A. Thompson[1], **G.H. Macdonald**[1], **and T.J. Millar**[2]

[1] Electronic Engineering Laboratory, University of Kent, Canterbury, Kent, CT2 7NT, UK
[2] Department of Physics, UMIST, P.O. Box 88, Manchester, M60 1QD, UK

Received 25 June 1998 / Accepted 3 November 1998

Abstract. We have undertaken a 330–360 GHz molecular line survey of the halo gas surrounding the hot core associated with G34.26+0.15. In contrast to our molecular line survey of the hot core itself, where 338 lines from at least 38 species were detected, only 18 lines from 9 species were detected in the halo. The lines are mainly single transitions of simple diatomic and triatomic molecules. Lower limits to their column densities have been evaluated by an LTE method. In the case of methanol, where four transitions were detected, the rotation temperature and column density have been evaluated by the rotation diagram technique. We have modified the previous depth-dependent chemical model developed in Paper II to calculate the column densities observed along a general line of sight drawn through the model cloud. The model is also extended to produce beam-averaged column densities for better comparison with those observed. We compare the model column densities with those observed and make recommendations for future depth-dependent chemical modelling of hot cores.

Key words: line: identification – ISM: abundances – ISM: individual objects: G34.3+0.15 – ISM: molecules – radio lines: ISM

1. Introduction

G34.26+0.15 is a complex of three HII regions 3.1 kpc from the Sun. Two of the H II regions are unresolved but the third is a spectacular cometary H II region 3″ wide with a clearly defined tail stretching for 20″ (Gaume et al. 1994). The whole complex is embedded in a molecular gas cloud approximately 3.5 × 4 pc with $n(\mathrm{H_2}) \sim 6 \times 10^3$ cm^{-3} (Heaton et al. 1985). Further molecular line observations (Martin-Pintado et al. 1985, Andersson 1985, Henkel et al. 1987, Matthews et al. 1987) inferred the presence of a hierarchical density structure within the cloud; a warm (225 K) compact core within the cloud surrounding in turn a more dense "ultracompact" core. Interferometric observations of G34.26+0.15 (Andersson & Garay 1986, Heaton, Little & Bishop 1989, Carral & Welch 1992) reveal an ultracompact (0.06 × 0.02 pc) core with $n(\mathrm{H_2}) \sim 4 \times 10^7$ cm^{-3}embedded in a compact (0.21 × 0.05 pc) core of density 6×10^5 cm^{-3}. The ultracompact core is located on the eastern edge of the cometary H II region and the interferometric observations of Heaton, Little & Bishop (1989) and Carral & Welch (1992) show that the compact core appears to be wrapped around the head of the cometary H II region (see Fig. 1).

The dense core associated with G34.26+0.15 bears a resemblance to the Orion Hot Core. They both share high abundances of saturated species, are dense compact clumps of gas, and are warm (100–200 K). These objects are known as "hot cores" (Walmsley & Schilke 1993) and are thought to be clumps of

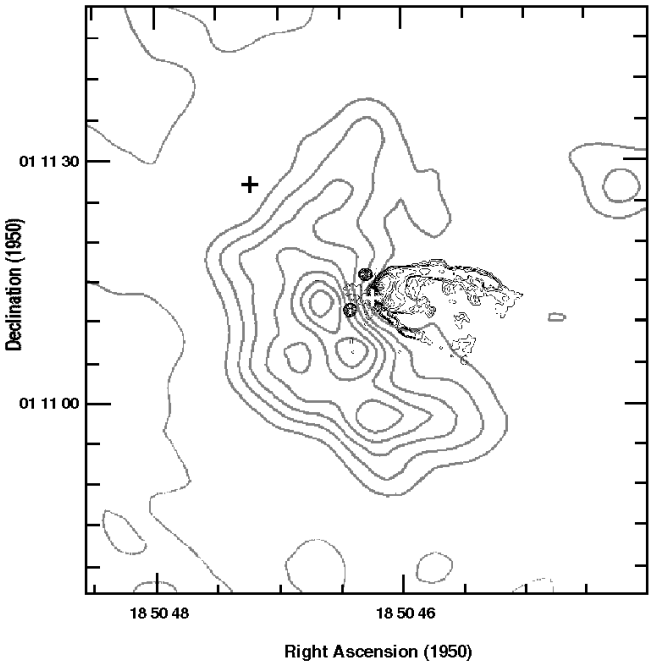

Fig. 1. Contour maps of G34.26+0.15 in molecular line emission and continuum. The black contours show the 2 cm continuum emission observed with the VLA by Gaume et al. (1994) and the grey contours show the HCO^+ J = 1→0 line emission observed with the BIMA-Hat Creek mm array by Carral & Welch (1992). The position used for the spectral survey of Paper I is marked with a white cross and the position of the halo spectral ssurvey described in this paper is marked by a black cross.

Send offprint requests to: G.H. Macdonald

gas left over from the formation of the massive star powering the H II region. The heat source responsible for warming the core is not yet fully understood. It may be an embedded source within the core itself (Wyrowski & Walmsley 1996, Olmi et al. 1996), arise from dynamical heating by molecular outflows or be simply due to radiation from the nearby massive star. Calculations of the energy balance in hot cores (Cesaroni et al. 1994) and radiative transfer modelling (Kaufman, Hollenbach & Tielens 1998) indicate that the former possibility is the most likely, however it is probable that all three processes are involved.

The relatively high gas temperature has a dramatic effect on the chemistry of the hot core. The switch-on of the heat source, be it an embedded protostar or a newly formed high mass star, evaporates ice mantles accreted on dust grains during the cold collapse phase of the cloud. The injection of the mantle molecules enriches the hot core chemistry. The high abundances of saturated species offer indirect evidence for grain mantle injection, as the relative mobilities of atoms within the grain mantles lead to hydrogenation being the most favourable grain surface chemical process. Observation and modelling of the chemistry within hot cores provides constraints upon the species injected into the gas phase, leading to a greater understanding of the chemical processes that occur in grain mantles.

In order to investigate the chemistry of hot cores Macdonald et al. (1996), hereafter Paper I, performed a spectral line survey of the hot core associated with G34.26+0.15. The survey covered the frequency range of 330–360 GHz, detecting 338 molecular lines which were subsequently identified as originating from at least 35 different chemical species. In conjunction with the spectral line survey of the hot core a detailed chemical model of G34.26+0.15 was developed (Millar et al. 1997, hereafter Paper II). Previous models of hot core chemistry (Millar et al. 1991, Charnley et al. 1992, Caselli et al. 1993, Charnley & Millar 1994, MacKay 1995 and Charnley et al. 1995) use a single point approach, i.e. the chemistry of the cloud evolves under conditions of constant density and temperature. The model of Paper II uses a structural model of the embedding cloud derived from molecular line observations (Heaton et al. 1989, 1993) to evaluate the physical conditions in a number of discrete concentric shells. The chemical evolution of each shell is followed by a reaction network containing 2184 separate reactions and the results from each shell are integrated along the line of sight to provide a radial chemical model of G34.26+0.15 as a function of time.

Observations of hot cores sample a column of gas through the cloud, encompassing both halo and core, averaging the column densities across the beam. The model of Paper II allows the chemical nature of each part of the structural model (halo, ultracompact and compact cores) to be analysed separately but has been constrained mostly by observations of the cores. We have undertaken a spectral line survey of the *halo* of G34.26+0.15 in the frequency range 330–360 GHz. We aim to characterise the cold gas phase chemistry of the halo, improve the predictions of the model of Paper II and test the predictions of the structural model against different molecular tracers. Our observations are described in Sect. 2 and the data reduction and analysis procedures are described in Sects. 3 and 4 respectively. The results of the radial chemical models are given in Sect. 5 and we discuss their implications and what can be done to enhance hot core chemical models in Sects. 6 and 7.

2. Observations

The observations were made with the James Clerk Maxwell Telescope (JCMT)[1] between the 8th and 14th March 1996. A position 20″ (0.3 pc) offset from the ultracompact core position was chosen to sample the halo gas. The coordinates of this position are $\alpha(1950) = 18\mathrm{h}\ 50\mathrm{m}\ 47.25\mathrm{s}$ and $\delta(1950) = 01^\circ\ 11'\ 27.0''$. This gives an offset from the ultracompact core of 14″ in α and 14″ in δ, or 0.3 pc at the assumed distance of G34.26 (3.1 kpc). The dimensions of the ultracompact and compact cores for comparison are 0.01 and 0.1 pc respectively. The pointing accuracy of the telescope was checked regularly against the peak continuum position of G34.26 itself. The pointing was found to be good to within 5″. The half power beam width of the JCMT at 345 GHz is 13″ and with an angular distance of only 20″ (and pointing errors of $\leq 5''$) from the hot core the possibility of picking up hot core gas in the edge of the beam (by pointing uncertainties or otherwise) or in the error beam ("sidelobes") must be considered. The former case is dealt with more fully in Sect. 5.2. For the latter case we note that the JCMT beam at 345 GHz is well modelled by an approximately circularly symmetric Gaussian and the peak amplitude of the sidelobes at this frequency is $< 6\%$ of the main beam peak amplitude. Error beam pickup of the core gas at this position should be negligible.

It was found that beam-switching (i.e. chopping the secondary mirror from on-source to off-source) was much superior to position switching for obtaining extremely flat baselines. A chop throw of 3′ in RA was used to keep a constant reference position, with a chopping frequency of 1 Hz. 3′ was more than sufficient to avoid contamination in the reference position for all species except CO (as can be seen in Fig. 2).

To cover the frequency range of the survey the 345 GHz SIS junction receiver B3i (RxB3i) was used in conjunction with the Dutch Autocorrelation Spectrometer (DAS). The DAS was used in 760 MHz bandwidth mode and with RxB3i as a frontend produces dual sideband spectra. Dual sideband spectra comprise two frequency bands (the upper and lower sidebands) folded over one another to produce a composite spectrum. The upper and lower sidebands are separated in frequency by approximately twice the local oscillator intermediate frequency (IF), depending on the doppler correction for the source velocity. The upper sideband frequency scale is also reversed relative to the lower sideband scale. The velocity of G34.26 with respect to the Local Standard of Rest (V_{LSR}) was assumed to be +58 km s^{-1}. For RxB3i the IF is 1.5 GHz and the upper and lower sidebands are separated by approximately 3 GHz. Each spectrum taken thus represents a total frequency range of ~ 1.5 GHz and this

[1] The JCMT is operated by the Royal Observatories on behalf of the Particle Physics and Astronomy Research Council of the UK, the Netherlands Organisation for Scientific Research and the National Research Council of Canada.

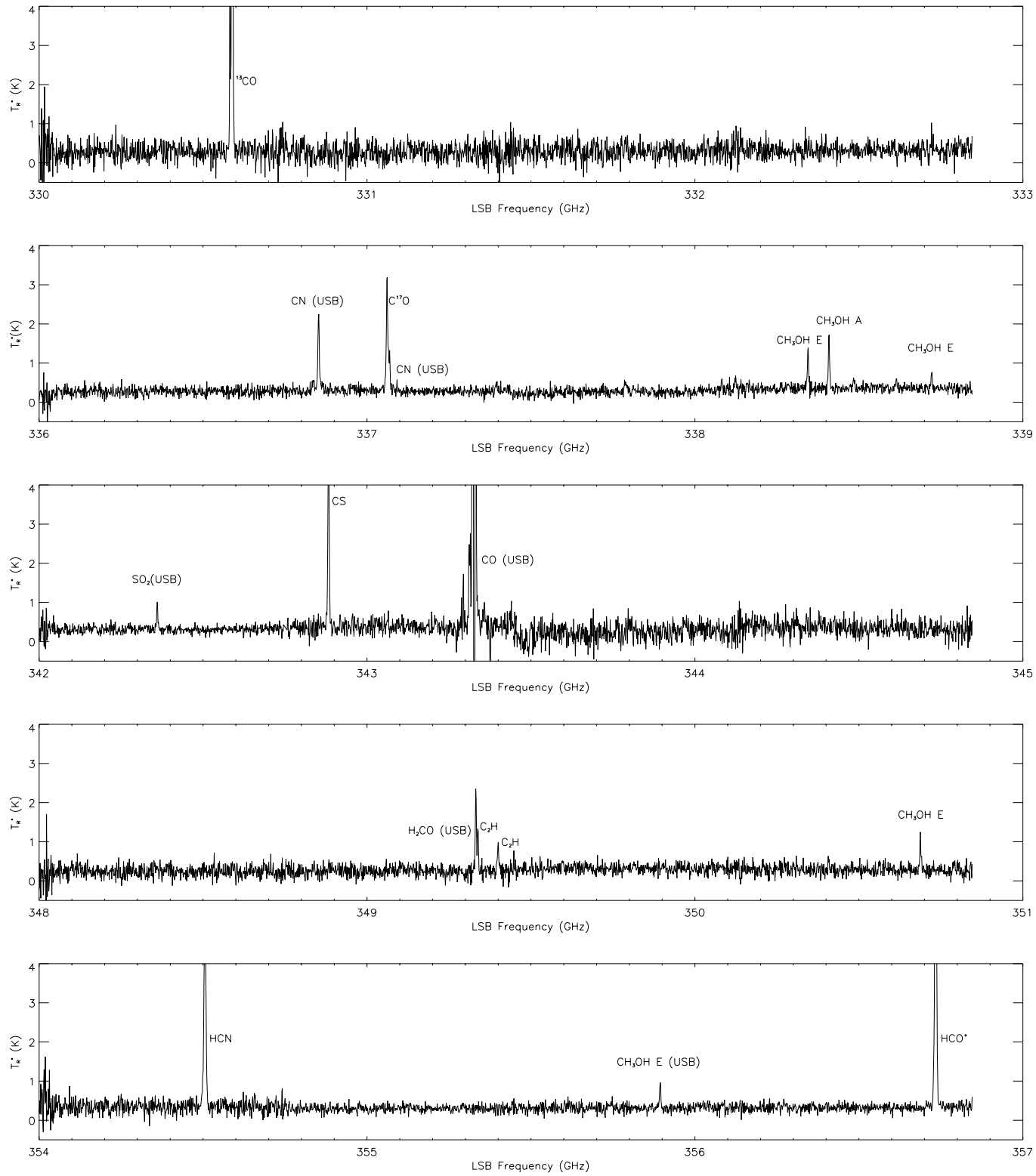

Fig. 2. Spectra observed during the 330–360 GHz survey of the halo of G34.26+0.15. The frequency scale given for each block of spectra is the lower sideband scale. The 10 MHz shifted spectra are not displayed and all spectra in a particular block have been concatenated. Upper sideband lines are indicated by USB, the frequencies of these lines do not correspond to the lower sideband scale. Species identifications are shown for each line. The H_2CO and C_2H lines are blended in the main spectra but the shifted spectra allows the separation of these two lines.

was used to reduce the total number of spectra needed to cover the frequency range of the survey.

The spectra were all observed with the "main band" set to the lower sideband, which means that the other (upper) sideband covers a frequency range of the same width roughly 3 GHz higher in frequency. We took spectra with their central frequency incremented by 700 MHz (ensuring an overlap of 30 MHz between spectra) until the lower sideband had covered the first 2.8 GHz of the frequency range. The upper sidebands of these spectra cover the next 2.8 GHz of the frequency range with a 200 MHz gap in coverage. This block of 4 spectra thus covers a total frequency range of 5.6 GHz. The remaining parts of the frequency range were observed in the same manner. The 200 MHz gaps between the blocks of spectra were to be covered by additional spectra taken at the end of the observing run, however due to bad weather this was not achieved. The blocks of spectra (with individual spectra concatenated) are shown in Fig. 2.

Two problems inherent in dual sideband spectra are the allocation of features to a particular sideband (i.e. upper or lower) and the possible overlapping (blending) of lines from each sideband. To determine the sidebands (and hence frequencies) extra spectra with a local oscillator shift of +10 MHz were taken. In the shifted spectra lines in the upper sideband will appear to shift frequency by 20 MHz relative to lines in the lower sideband. Blended lines from both sidebands were separated by this technique whenever possible.

With the DAS in 760 MHz mode the spectral resolution is 0.756 MHz. Each spectrum was divided into channels of 0.625 MHz, although later in the data reduction process all spectra were binned to a channel width of 1.25 MHz to improve signal to noise. The standard chopper-wheel calibration method of Kutner & Ulich (1981) was used to obtain line temperatures on the T_A^* scale, i.e. corrected for the atmosphere, resistive telescope losses and rearward spillover and scattering. T_A^* can also be corrected for forward spillover and scattering to give the corrected receiver temperature T_R^* where $T_R^* = T_A^*/\eta_{fss}$ and η_{fss} is the forward spillover and scattering efficiency (0.7 for the JCMT at 345 GHz). All line temperatures quoted in this paper are on the T_R^* scale, unless otherwise indicated.

3. Data reduction and line identification

3.1. Data reduction

The data were reduced using the Starlink spectral line package SPECX. Linear baselines were subtracted from the spectra and the line parameters of peak temperature (T_A^*), central frequency ($\nu(\mathrm{obs})$) and line width at half maximum ($\Delta\nu_{1/2}$) were measured. Values for the noise in the spectra were evaluated using line-free channels and the typical rms noise level was found to be $\sigma \sim 0.1$ K. Features below the detection limit of 5σ were ignored to avoid inaccurate line identifications. It should be noted that only one feature below 5σ was seen which was tentatively identified as the 7(8)–6(7) line of SO, however the line was very weak with a peak temperature of only 0.2 K and has been neglected from any further analysis. These data are given in Table 1 for each line. Multiple independent detections of each line are listed (i.e. from both the main and the 10 MHz shifted spectra). Self-absorbed lines have been excluded from the analysis and are indicated as such in Table 1.

3.2. Line identification

Eighteen lines from 11 species (including isotopomers) were detected in this survey. The lines were identified by comparing their central frequencies to those of the lines detected in the spectral line survey of Paper I. The spectral line lists used to identify the lines in Paper I include Lovas (1992), Poynter & Pickett (1985), Anderson, Herbst & De Lucia (1993) and the observational list of lines seen by Jewell et al. (1989) towards Orion-KL. The identified lines are listed in Table 1. All our detected lines were identified with those also seen at the central position of Paper I.

4. Analysis

The lines identified in this survey have been analysed using the LTE method of Turner (1991). For optically thin emission from molecules in LTE the column density (N_{mol}) can be written as

$$N_{\mathrm{mol}} = \frac{3k}{8\pi^3}\frac{\int T_R \mathrm{d}v}{\nu S\mu^2 g_I g_K} Q(T_{\mathrm{rot}})\exp\left(\frac{E_{\mathrm{u}}}{kT_{\mathrm{rot}}}\right) \quad (1)$$

where $\int T_R \mathrm{d}v$ is the integrated intensity of the line, ν is the line frequency, S is the line strength, μ is the permanent electric dipole moment, g_I and g_K are the reduced nuclear spin degeneracy and the K-level degeneracy of the molecule respectively. E_u is the energy of the upper level of the line and T_{rot} is the rotational temperature of the molecules. The integrated intensity of each line has been calculated using $\int T_R \mathrm{d}v = 1.06 T_A^* \Delta v_{1/2}/\eta_{fss}$, where the line is assumed to be gaussian in shape. The partition functions used are interpolated from the values given in the JPL molecular line database (Poynter & Pickett 1985).

We have used Eq. 1 in two different forms, to put lower limits on the column densities of molecules with one or two detected lines and where possible to constrain the temperature and column density of the gas with the rotation diagram method. All column densities quoted in this paper are beam averaged.

4.1. Rotation diagram analysis

Eq. 1 may be rearranged to give

$$\log_{10}(L) = \log_{10}\left(\frac{N_{\mathrm{mol}}}{Q(T_{\mathrm{rot}})}\right) - \frac{E_u}{k}\frac{\log_{10}e}{T_{\mathrm{rot}}} \quad (2)$$

where $L = (3k\int T_R \mathrm{d}v/8\pi^3\nu S\mu^2 g_I g_K)$. If Eq. 2 is plotted with E_{u} as abscissa and $\log_{10}(L)$ as ordinate it is the equation of a straight line with a gradient of $-\log_{10}e/kT_{\mathrm{rot}}$ and a y-intercept of $\log_{10}(N_{\mathrm{mol}}/Q(T_{\mathrm{rot}}))$. These parameters have been determined by least-squares fitting of a straight line to the data. The errors in N_{mol} and T_{rot} originate from the uncertainty in the integrated intensity of the line ($\int T_R \mathrm{d}v$) which has been plotted as error bars on the rotation diagram (Fig. 3).

Table 1. The measured line parameters of observed frequency (ν(obs)), peak temperature (T_R^*) and line width ($\Delta\nu_{1/2}$) for each detected line are listed here. Multiple detections of the same line have been included. Lines that are blended are indicated in the Notes column by *blended* if they are blended with a different species or *hyperfines* if they are a mixture of two or more hyperfine components. Self-absorbed lines are also listed.

ν(obs) (GHz)	T_R^* (K)	$\Delta\nu_{1/2}$ (MHz)	Species	Transition	ν(rest) (GHz)	Notes
330.586			^{13}CO	3–2	330.5879	self-absorbed
330.586			^{13}CO	3–2	330.5879	self-absorbed
330.586			^{13}CO	3–2	330.5879	self-absorbed
337.061	2.73	4.1	C^{17}O	3–2	337.0611	
337.062	2.93	5.0	C^{17}O	3–2	337.0611	blended
338.345	1.05	4.0	CH_3OH	7(-1)–6(-1) E	338.3446	
338.345	1.40	2.8	CH_3OH	7(-1)–6(-1) E	338.3446	
338.409	1.38	3.3	CH_3OH	7(0)–6(0) A+	338.4088	
338.408	1.58	3.9	CH_3OH	7(0)–6(0) A+	338.4088	
338.722	0.43	2.8	CH_3OH	7(2)–6(2) E	338.7216	
338.722	0.45	2.8	CH_3OH	7(2)–6(2) E	338.7216	
340.031	1.04		CN	3–2 2.5 2.5–1.5 1.5	340.0355	blended & hyperfines
340.032	0.91	7.1	CN	3–2 2.5 2.5–1.5 1.5	340.0355	hyperfines
340.033	1.33	7.5	CN	3–2 2.5 2.5–1.5 1.5	340.0355	hyperfines
340.033	1.05	8.2	CN	3–2 2.5 2.5–1.5 1.5	340.0355	hyperfines
340.247	1.98	5.2	CN	3–2 3.5 3.5–2.5 1.5	340.2478	hyperfines
340.248	1.89	5.2	CN	3–2 3.5 3.5–2.5 1.5	340.2478	hyperfines
340.248	2.16	6.0	CN	3–2 3.5 3.5–2.5 1.5	340.2478	hyperfines
340.248	2.22	4.9	CN	3–2 3.5 3.5–2.5 1.5	340.2478	hyperfines
342.882	4.21	5.1	CS	7–6	342.8829	
342.882	4.49	6.2	CS	7–6	342.8829	
342.882	4.12	3.9	CS	7–6	342.8829	
342.883	4.74	4.0	CS	7–6	342.8829	
345.339	0.71	3.4	SO_2	13(2,12)–12(1,11)	345.3385	
345.794			CO	3–2	345.7959	self-absorbed
345.794			CO	3–2	345.7959	self-absorbed
349.338	1.10	4.0	C_2H	4.5–3.5	349.3381	
349.339	1.11	5.1	C_2H	4.5–3.5	349.3381	
349.400	0.75	3.5	C_2H	3.5–2.5	349.4006	
349.400	1.05	4.5	C_2H	3.5–2.5	349.4006	
350.688	0.98	2.3	CH_3OH	4(0)–3(1) E	350.6877	
350.688	0.90	5.1	CH_3OH	4(0)–3(1) E	350.6877	
351.768	2.13	4.0	H_2CO	5(1,5)–4(1,4)	351.7686	
351.768	2.11	4.0	H_2CO	5(1,5)–4(1,4)	351.7686	
354.506	4.92	7.1	HCN	4–3	354.5061	
354.506	5.03	7.1	HCN	4–3	354.5061	
356.734	8.78	6.2	HCO^+	4–3	356.7342	
356.734	8.93	6.3	HCO^+	4–3	356.7342	
358.606	0.65	3.3	CH_3OH	4(1)–3(0) E	358.6058	
358.605	0.66	3.3	CH_3OH	4(1)–3(0) E	358.6058	

Care must be taken with the rotation diagram approach. As noted in the previous section the underlying assumptions are that the gas is in LTE, is optically thin and can be characterised by a single temperature. Optically thick emission will affect the temperature derived from the rotation diagram, in some cases lowering the derived temperature or mimicking a two-component temperature distribution (e.g. Serabyn & Weisstein 1995).

The only molecule in our survey with sufficient detected lines for a rotation diagram to be constructed is methanol (CH_3OH). The lines of methanol are fairly weak ($\leq$ 1 K) and are expected to be optically thin. There is a possibility that the methanol lines are picked up in the fringes of the telescope beam and may originate from the core, where they exhibit optical depths of roughly 10 (Hatchell et al. 1998a). The linewidths of the lines seen in the halo survey are much narrower than those seen in the hot core survey of Paper I (an average of 3 MHz in the halo survey as opposed to 9 MHz in the hot core survey), suggesting that they originate from the colder gas of the halo and

Table 2. Assumed excitation temperature and lower limits to column density for molecules with one or two detected lines. The third column contains the corresponding values of column density observed toward the centre of the cloud from Paper I. The values for SO_2 and A-type CH_3OH had sufficient detected transitions to form rotation diagrams and their rotation temperatures (in brackets) and column densities are given. Other species in the core had only one or two detected transitions and the core column densities are lower limits for these species. The SO_2 rotation diagram from Paper I was evaluated for lines with $E_u/k < 250$ K.

Molecule	T_{ex} (K)	Outer Halo N_{min} (cm^{-2})	Cloud centre N_{min} (cm^{-2})
$C^{17}O$	32	$> 5.4 \times 10^{15}$	$> 1.2 \times 10^{16}$
C_2H	42	$> 2.9 \times 10^{14}$	$> 8.1 \times 10^{15}$
CN	33	$> 9.5 \times 10^{12}$	$> 5.9 \times 10^{14}$
CS	66	$> 5.3 \times 10^{13}$	$> 8.4 \times 10^{13}$
H_2CO	62	$> 1.3 \times 10^{14}$	$> 1.7 \times 10^{14}$
HCN	43	$> 2.3 \times 10^{13}$	$> 3.8 \times 10^{13}$
HCO^+	43	$> 2.3 \times 10^{13}$	$> 7.2 \times 10^{14}$
SO_2	62	$> 2.0 \times 10^{14}$	$(108 \pm 4$ K$)$ $1.6 \pm 0.2 \times 10^{15}$
CH_3OH A-type	43	$> 3.6 \times 10^{14}$	$(368 \pm 16$ K$)$ $1.8 \pm 0.2 \times 10^{16}$

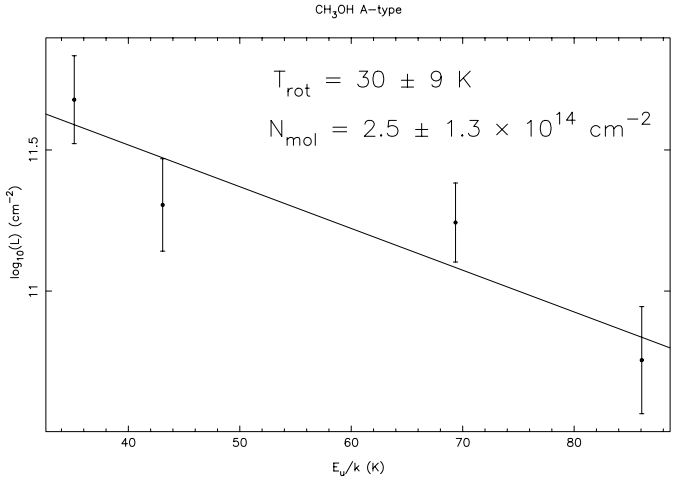

Fig. 3. Rotation diagram of the methanol E-type lines detected in the halo of G34.26+0.15. The rotation temperature and column density evaluated from Eq. 2 are indicated on the diagram.

not the core. We can be reasonably confident that the methanol emission originates from the halo and is likely to be optically thin, i.e. the rotation diagram approach is valid and the results of the analysis should not be affected by pick-up of the hot core gas.

Methanol possesses two different forms, the A and E-types, which must be analysed separately. Four lines of CH_3OH E-type were detected and a rotation diagram yields a rotation temperature $T_{rot} = 30 \pm 9$ K and a column density N_{mol} = 2.5 $\pm 1.3 \times 10^{14}$ cm^{-2} (as shown in Fig. 3). This compares with the values from the central position of Paper I of $T_{rot} = 336 \pm 14$ K and $N_{mol} = 1.9 \pm 0.1 \times 10^{16}$ cm^{-2}. The A-type form of methanol was detected in only one line and has been analysed using the column density lower limit method described in the next section.

4.2. Lower limits to column density for molecules with one or two detected lines

For molecules with only one or two detected lines we have employed a modification of Eq. 1 to determine a lower limit to the column density, N_{min}. To evaluate the rotational temperature we set the derivative of the temperature dependent part of Eq. 1 to zero, i.e. $\frac{d}{dT_{rot}}(Q(T_{rot})exp(E_u/kT_{ex})) = 0$, where $Q(T_{ex})$ is the appropriate partition function for each molecular type. It can be shown that for linear molecules $T_{ex} = E_u/k$ and for symmetric and asymmetric top molecules $T_{ex} = 2E_u/3k$. Forming the second derivative shows that these turning points are minima and hence N_{min} can be found as shown in Eq. 3.

$$N_{min} = \frac{3k}{8\pi^3}\frac{\int T_R dv}{\nu S\mu^2 g_I g_K} Q(E_u/k)e \qquad (a)$$
$$N_{min} = \frac{3k}{8\pi^3}\frac{\int T_R dv}{\nu S\mu^2 g_I g_K} Q(2E_u/3k)e^{2/3} \quad (b) \qquad (3)$$

where form *(a)* is used for linear molecules and form *(b)* is used for symmetric and asymmetric tops. This analysis was performed for the remaining molecular lines in our survey. Again care must be taken that the lines are optically thin and in LTE. High optical depth will underestimate the integrated intensity of the line, reducing the "correct" estimate of N_{min}. As N_{min} is a lower limit to the column density it follows that in cases of high optical depth the lower limit will be reduced, but will however still be a lower limit to the column density of the gas. The column density lower limit (N_{min}) and assumed excitation temperature (T_{ex}) are summarised in Table 2 alongside the corresponding values from Paper I.

5. Comparison with the chemical model of Paper II

The chemical model of Paper II represents an improvement on previous single-point time-dependent chemical models of hot cores by basing the chemical evolution of the gas around a physical and structural model of the cloud deduced from molecular

Table 3. Physical parameters of the structural model for G34.26+0.15 developed by Heaton et al. (1989)

Component	nH_2 (cm^{-3})	T (K)	Outer radius (pc)	N(H_2) (cm^{-2})
ultracompact core	2×10^7	300	0.01	6×10^{23}
compact core	10^6	$30r^{-0.4}$	0.1	2.7×10^{23}
halo	$10^4 r^{-2}$	$30r^{-0.4}$	3.5	2.9×10^{23}

line observations (Heaton et al. 1989, 1993). The physical model divides the cloud into three spherical components: an ultracompact core of temperature 300 K and density 2×10^7 H_2 molecules per cm^3, a surrounding compact core with temperature falling as $r^{-0.4}$ K and density 10^6 H_2 molecules per cm^3, all embedded within a large halo 3.5 pc in radius with temperature falling as $r^{-0.4}$ K and density falling as r^{-2} H_2 molecules per cm^3. The parameters of the physical model are summarised in Table 3.

The chemical model uses the values derived from the physical model to evaluate the temperature and density at 22 radial points within the model cloud. The innermost 3 points overlap to some degree and the cloud model thus contains 19 concentric "shells" of constant temperature and density. The structural model predicts that the physical conditions within the ultracompact and compact cores change relatively little from centre to edge. The ultracompact and compact cores are thus represented by a single shell each. The halo, where the conditions from inner edge to outer edge are very different, is modelled by the remaining 17 shells. Within each shell the chemical evolution is followed by a reaction network containing 225 species and 2184 separate reactions. The reaction network includes evolution from atomic gas and grain evaporated species.

The choice of method used to compare the model predictions with the observations is limited by the critical assumptions of both the analysis of the observational data and the chemical model. We outline the major assumptions of the analysis procedure and the chemical model below. The comparison of the model to the observations is also explained, as are the main caveats.

The main assumptions in our analysis of the observational data is that the gas is in LTE, optically thin and characterised by a single (rotational) temperature. For molecules with a high critical density (e.g. CS) the density of the halo may not be sufficient to thermalise the transitions and the assumption of LTE may break down. We are reasonably confident that most detected transitions are optically thin, the lines (with the exception of CO and ^{13}CO) do not exhibit self-absorption. The more optically thin isotopomers of certain lines (e.g. C^{34}S, ^{34}SO2, H^{13}CN) are not detected down to the noise level, indicating that at *most* the optical depths are of the order 2–3. The results from the analysis yield lower limits to the column density for most molecules, with methanol being the only species for which a strict temperature and column density could be derived.

The structural model upon which the chemical model is based assumes a spherical geometry for the cloud which clearly is not the case in reality (Fig. 1). However we note that the structural model on which the chemical model is based (Heaton et al. 1993) reproduces the observed line profiles extremely well by assuming spherical geometry. The column densities of the core in Millar et al. 1997 are calculated by mutiplying the fractional abundances produced by the chemical model by the appropriate cloud densities generated by the physical model and integrating along the line of sight through the core. These column densities depend upon the cloud geometry, and as the integration extends through the full depth of the cloud the emission is implicity assumed to be optically thin. The evolution timescales are dependent upon the initial abundances of the model, which for the halo arbitrarily consist of atomic gas (see Millar et al. 1997 for further details). The timescales for the halo derived from various species should thus not be taken too literally but in the absence of a more rigorous model (perhaps combining the physical and chemical evolution of the cloud) at least the broad timescales of the halo can be determined.

Given these difficulties in interpretation we have decided to follow the simplest means of comparing the model predictions to the observations by contrasting the predicted and observed column densities. Although our simple method does not take account of possibly optically thick emission and limits to column density the approach undertaken is important. With the advent of hot core chemical models that couple the chemistry to the physical conditions throughout the cloud rather than just at a single point, the questions of beam-averaging by the telescope, radiative transfer and the physical evolution of the cloud become extremely relevant. We aim to take the current single-point chemical models a step further by adding the concept of cloud structure (Paper II) and the beam-averaging effect of the telescope (this work). Comparison of the model predictions with the observations points to further improvements that can be made in the modelling process (such as the addition of radiative transfer, see Sect. 7) and identifies the need for further observations to constrain the observed column densities and provide additional data for more rigorous modelling of the halo and core.

Paper II concentrated on the model predictions for the column density observed along a central line of sight through the cloud, i.e. a "point" column density observed at the centre of the cloud. Here we extend and adapt the model to predict the column densities observed at an offset position within the halo and compare these predicted column densities with our observed values. We have adopted two approaches: a single line of sight drawn through the cloud much like the method used in Paper II and a beam-averaged approach, weighting multiple lines of sight drawn through the cloud with a gaussian to approximate the sampling effect of the telescope beam.

The "pencil-beam" single line of sight approach is illustrative to compare with the extended beams used in the beam-averaged model and the observations. Previous chemical models of hot cores have all relied on the single-point approach. It is interesting to see just how the beam-averaging process affects a single point model, i.e. how effective the single-point models were at predicting the beam-averaged observations. In addition there is an important difference between these two approaches. The "pencil-beam" drawn through the model cloud correspond-

ing to the position of the halo survey does not intersect the cores and the column densities predicted by this model are representative of the halo chemistry alone. The beam-averaged model on the other hand is comprised of multiple lines of sight, some of which do intersect the core gas. The beam-averaged model shows that the effect of the core chemistry may extend to influence our observations made of the halo. By comparing the two approaches we can test whether the model halo chemistry alone can reproduce the observed column densities, or whether the areas of the core covered by the fringes of the telescope beam still dominate the observed column densities. Each approach is described in more detail in the following two sections.

5.1. Single line of sight model

Our first method of interpreting the radial chemical model of G34.26+0.15 was to evaluate the column densities along a "pencil-beam" line of sight corresponding to the centre of the telescope beam of our halo spectral line survey, i.e. 20″ or 0.3 pc from the centre of the cloud. It is a useful approach to compare the "pencil-beam" model with the extended beam of the observations because all previous models of hot cores have been single point (and thus pencil-beam models). Comparing the two models with the extended beam of the observations allows us to assess how effective a single point model is at predicting the column densities.

A diagram of the model is shown in Fig. 4, indicating some of the shells and their depths along the line of sight, radii, fractional abundances and densities (d_i, r_i, f_i and ρ_i respectively). The shell depths along the line of sight (d_i) are evaluated geometrically as shown in Fig. 4. The density of each shell is calculated from the structural model and the fractional abundances of each species are taken from the chemical model of Paper II. The product of the fractional abundance of each species and the density of the gas within the shell gives the number density of each species within each shell. The depth of each shell is then used to obtain the column density of each species by integrating along the line of sight. The full thickness of the cloud along the line of sight is taken into account, which implicitly assumes that the emission from the species considered is optically thin.

To contrast our observations with the model predictions we have used models with halo ages of 10^4, 10^5 and 10^6 years. We have compared the ratios of column density predicted by the model and that observed in our survey; these ratios can be seen in Table 4. The best fit to the observations is given by the model with a halo age of 10^6 years, although it can be seen that for many of the molecules seen in the survey (e.g. CN, CS, H_2CO and HCN) the model predicts a $\sim$ 10–300 times greater column density than is observed.

Different molecules appear to predict different ages; i.e. the CO column density ratio is favoured by an older halo of 10^6 years whilst the SO_2 column density ratio has a good fit to a halo of between 10^4 and 10^5 years with older halos possessing a much larger column density of SO_2 than is observed towards G34.26+0.15. CH_3OH is another molecule whose predicted column density favours a younger halo of between 10^4 and 10^5 years, as the column density of CH_3OH falls rapidly as the halo increases in age.

Table 4. The ratio of model column density to observed column density for each model calculated with the single line of sight approach. The ratio for CO is calculated with the observed column density of $C^{17}O$ assuming the $^{16}O/^{17}O$ ratio of 2400. Observed column densities are lower limits with the exception of CH_3OH.

Species	Model/Observed N_{mol} ratio for Halo Ages		
	10^4 years	10^5 years	10^6 years
CO	0.184	0.661	0.733
C_2H	19.3	8.13	0.228
CN	416	315	46.2
CS	426	1053	305
H_2CO	47.7	46.9	9.76
HCN	329	43.6	9.85
HCO^+	31.2	67.7	59.2
SO_2	0.015	10.2	92.5
CH_3OH	1.97	0.304	0.009

We must reconcile the apparently different ages predicted by the single line of sight model. The single line of sight model represents only the cold gas-phase chemistry of the halo. However, our observed column densities are averaged across the telescope beam which is of finite size unlike the "pencil-beam" single line of sight drawn through the cloud. The telescope beam samples an area of the cloud which will include both warmer gas closer towards the core and colder gas further away from the core. The grain mantle evaporation chemistry of the hot dense gas in the cores is significantly different from the cold gas-phase chemistry of the halo. The column densities of species picked up in the fringes of the telescope beam will thus affect the overall beam-averaged column density. There is some evidence for this in the observations, the linewidths of HCN and CS in the halo are similar to their linewidths in the core. The linewidths of the other species are much less (typically half or a third of the core linewidth) which suggests that they originate mainly from the cooler gas of the halo. In the next section we describe a multiple line of sight approach to interpreting the model which attempts to simulate the beam-averaging effect of the telescope.

5.2. Beam-averaged model

As described above the single line of sight method does not reproduce accurately the CO column densities observed in the halo. The halo column densities observed in this survey may also have a contribution from the gas close to the cores. Our observations were carried out with a 13″ beam and 20″ offset from the central position of Paper I. At the distance of G34.26 (3.1 kpc) this is equivalent to an HPBW of 0.2 pc and an offset of 0.3 pc (the radius of the compact core is 0.1 pc for comparison). For a gaussian beam of this HPBW the distance at which the beam falls to the 1% level is 0.25 pc. In a simple one dimensional beam we can see that, considering the 1% level as a "cutoff", there is still a 0.05 pc overlap with the compact core (which has a

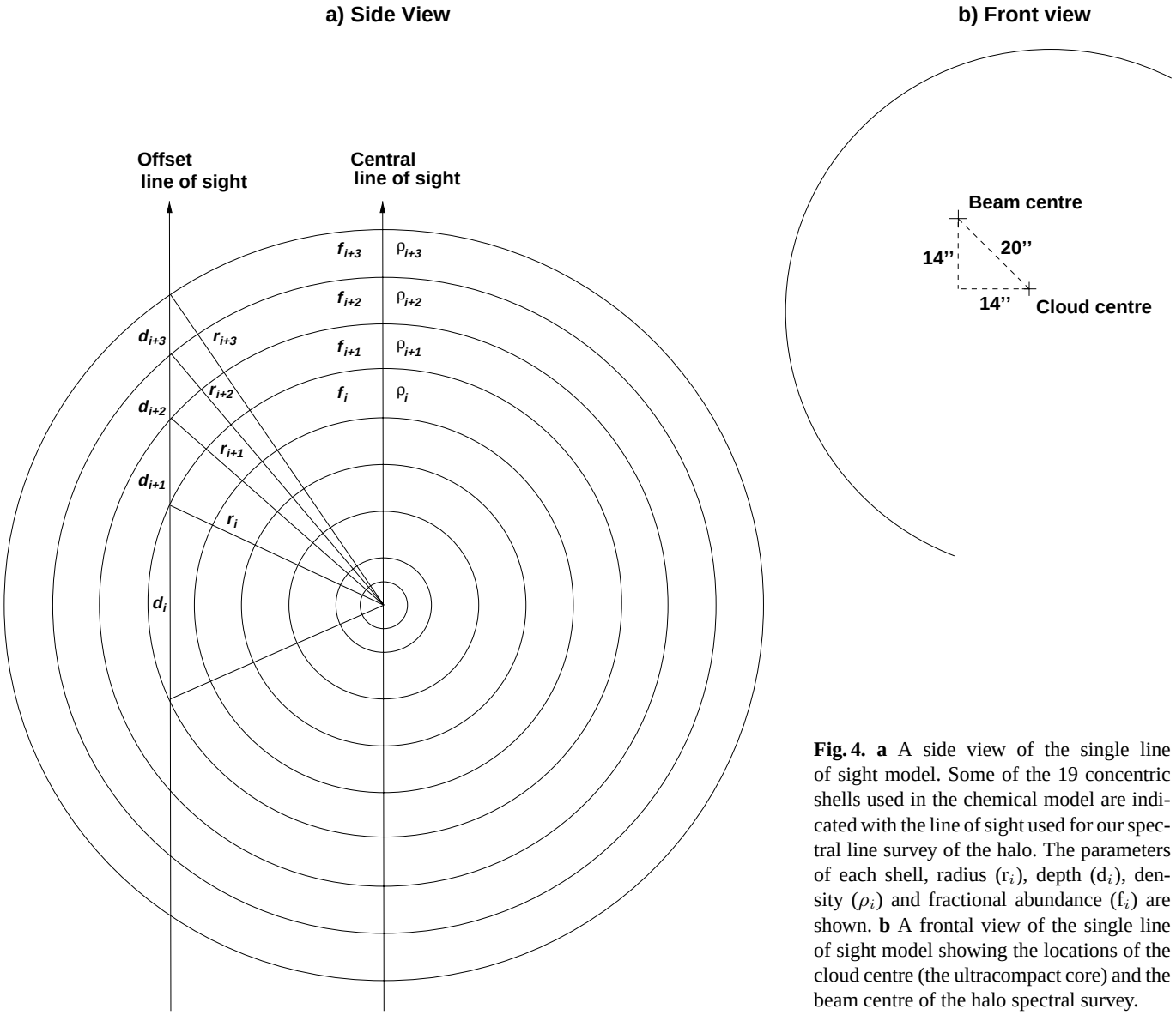

Fig. 4. a A side view of the single line of sight model. Some of the 19 concentric shells used in the chemical model are indicated with the line of sight used for our spectral line survey of the halo. The parameters of each shell, radius (r_i), depth (d_i), density (ρ_i) and fractional abundance (f_i) are shown. **b** A frontal view of the single line of sight model showing the locations of the cloud centre (the ultracompact core) and the beam centre of the halo spectral survey.

radius of 0.1 pc). The column densities seen in the compact core for some species are between 2–3 orders of magnitude greater than in the halo. It is plausible that the dense gas of the cores sampled in the edge of the beam contributes roughly the same amount (or possibly more) towards the beam-averaged column density as does the halo gas.

Pointing offsets during the observations may exacerbate the problem of core pickup. The estimated maximum offset during the observations was 5″, if it is assumed that the offset was toward the core then the beam centre will move 0.08 pc closer toward the core and the overlap with the compact core becomes 0.13 pc. However it is also likely that the pointing offsets could move the beam centre as far away from the core, negating the overlap entirely. As mentioned in the previous section, there is some evidence for core pickup in the observed linewidths of certain species (HCN and CS). This is not the case for the remaining species which have narrower halo linewidths than core linewidths. Once the structure of the cloud is taken into account by the chemical model it is important to consider the spatial sampling of the telescope and so to simulate the beam-averaged column density that the JCMT "sees" we have extended the single line of sight technique to include beam-averaging.

We use a square grid of equally spaced points centred on the beam centre, extending to the one percent level of a gaussian function corresponding to the telescope beam, to give the locations of the lines of sight to be drawn through the cloud. We have experimented with different levels of sampling the model to approximate to the JCMT beam of 13″ HPBW at 345 GHz. A relatively coarse level of sampling was first used with a separation between grid points of 0.1 pc and a 7×7 grid. This proved to have reasonable model run times but did not adequately sample the core gas where the dimensions are 0.01–0.1 pc (i.e. $\leq$ the grid spacing). A grid spacing of 0.01 pc (53×53 grid points) was found to be a good compromise between run time and sampling

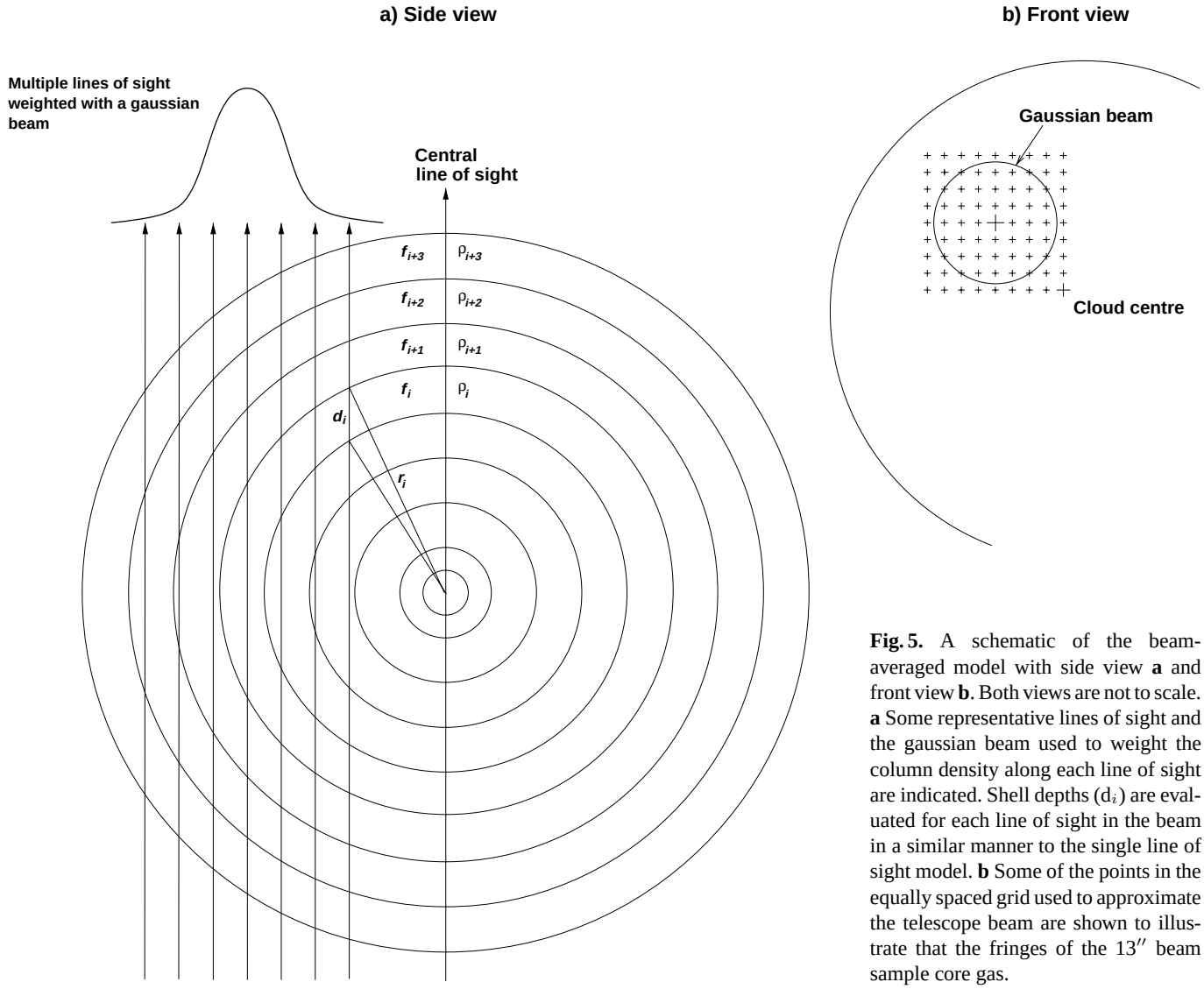

Fig. 5. A schematic of the beam-averaged model with side view **a** and front view **b**. Both views are not to scale. **a** Some representative lines of sight and the gaussian beam used to weight the column density along each line of sight are indicated. Shell depths (d_i) are evaluated for each line of sight in the beam in a similar manner to the single line of sight model. **b** Some of the points in the equally spaced grid used to approximate the telescope beam are shown to illustrate that the fringes of the 13″ beam sample core gas.

level. Decreases in the grid spacing below 0.01 pc have little effect on the beam-averaged column densities. A schematic of the beam-averaged model is given in Fig. 5. The gaussian beam corresponding to the telescope beam is used to obtain the appropriate weight for each line of sight and the weighted lines of sight are summed over the beam to give beam averaged column densities.

We have calculated the ratios for a combination of twelve models with 4 different core ages (3.2×10^2, 10^3, 3.2×10^3 & 10^4 years) and 3 different halo ages (10^4, 10^5 & 10^6 years). Model fits to the observations for each halo age and the oldest and youngest core ages are shown in Table 5.

From the results displayed in Table 5 it can be seen that on the whole the beam-averaged model does not produce significantly different results to the "pencil-beam" model. The column densities of most species are roughly 6–7% greater than the pencil-beam model, attributable to the beam-averaged H_2 column density being greater than the "pencil-beam" H_2 column density by roughly 7%. However some molecules have a difference much greater than 7% which is evidence that the warmer gas in the fringes of the beam does affect the beam-averaged column densities (at least in the model). The clearest example of this is methanol, which in the old halo of $\sim 10^6$ years has a model column density raised by a factor of ~ 400 compared to the single line of sight model.

The evolution of the core gas has little effect as the column density ratios of most molecules remain unchanged over the timescales of the core evolution. The ratios of CH_3OH, SO_2 and HCN are modified from the single line of sight model prediction when core evolution is taken into account. The model column density CH_3OH falls by roughly a factor of two as the core ages from $3.2 \times 10^2 \rightarrow 10^4$ years, the SO_2 column density rises sharply for core evolution with a halo of 10^4 years and the HCN column density rises marginally over all the halo ages, with the largest increase at a halo age of 10^6 years.

CO again predicts a halo age of 10^5–10^6 years, as do the molecules C_2H and H_2CO. Other molecules are over-estimated in the old halo by factors of 10–300. CH_3OH gives an uncertain

Table 5. The ratio of model column density to observed column density for each model calculated with the beam-averaged approach. We have also included the youngest and oldest core models to illustrate the effects of core evolution on the beam-averaged column density. The ratio for CO is calculated with the observed column density of $C^{17}O$ assuming the $^{16}O/^{17}O$ ratio of 2400. Observed column densities are lower limits with the exception of CH_3OH.

Halo Age	10^4 years		10^5 years		10^6 years	
Core age	3.2×10^2 years	10^4 years	3.2×10^2 years	10^4 years	3.2×10^2 years	10^4 years
CO	0.203	0.203	0.711	0.711	0.785	0.785
C_2H	20.1	20.1	8.24	8.25	0.237	0.244
CN	436	437	320	320	47.4	47.6
CS	452	453	1117	1119	317	318
H_2CO	50.8	50.8	49.9	49.9	3.11	3.14
HCN	350	358	45.0	53.1	10.4	18.5
HCO^+	33.3	33.3	72.2	72.2	63.2	63.2
SO_2	0.017	5.00	11.38	16.36	94.9	99.9
CH_3OH	6.43	4.42	4.65	2.63	4.35	2.33

prediction since its column density is affected by the core evolution, from the CH_3OH evidence alone any halo age is plausible. SO_2 is over-produced in the model cloud at late halo ages by a factor of 10–100, the best prediction of the cloud age using SO_2 is for a young halo of 10^4 years with a core age of between 3.2×10^3 and 10^4 years. We will interpret these and the single line of sight results in the next section.

6. Discussion

Comparing the two models allows us to contrast the gas-phase halo chemistry sampled by the single line of sight model and the mixed gas-phase and mantle-evaporation chemistry sampled by the beam-averaged model. In particular it will allow us to determine the most probable origins of certain species, i.e. can the observed column densities be reproduced by gas-phase chemistry alone or do they depend upon the grain mantle-evaporation chemistry sampled in the fringes of the beam? The limitations of the column densities derived from the observations and the predictions of the model have already been mentioned in Sect. 5; in this section we dwell upon them in more detail. We will interpret the predictions of our models below and discuss what can be done to enhance the chemical modelling of hot cores, in particular the radial chemical model of G34.26+0.15, in the next section.

Firstly, what are the similarities between both models? Broadly speaking the ratios of the model to observed column density are fairly similar in both models for most molecules (CH_3OH is the notable exception, as is SO_2 when core evolution is considered). The column densities predicted by the beam-averaged model are higher than the corresponding column densities predicted by the single line of sight model, which is due to the beam-averaged column density being larger than the "pencil-beam" column density by roughly 7%. In the early halo both models do not predict sufficient CO (by a factor of up to 5) and overestimate the column densities of the other species by factors of up to several hundred at early halo ages. The model values when compared to the observations suggest a halo age of 10^6 years (apart from CH_3OH, SO_2 and to a lesser extent HCO^+). The column densities of CS are not well reproduced by either model.

Secondly, what are the differences between the single line of sight model and the beam-averaged model? The only molecule for which the inclusion of beam-averaging significantly alters the column density at all times in the model is CH_3OH. The methanol in the halo alone decays rapidly over the timescale of the halo evolution whereas in the beam-averaged case the methanol abundance remains roughly constant. The chemical evolution of the core tends to have little effect upon the column densities of most molecules, but the column densities of CH_3OH and SO_2 change over the core evolution timescale. The CH_3OH column density is reduced by a factor of almost 2 as the core evolves from 3.2×10^2 to 10^4 years. The column density of SO_2 is strongly affected by the core evolution in the early halo (the model/observed ratio changes from $0.017 \rightarrow 5.00$). This occurs because relatively little SO_2 is initially present in the halo gas but is formed in core gas as H_2S is broken down. At older times in the halo, SO_2 is made efficiently and the core makes a difference to the total column density at the 5% level (at a halo age of 10^6 years the model/observed ratio changes from $94.9 \rightarrow 99.9$). HCN is also slightly affected by the evolution of the core with the greatest change occurring with a halo age of 10^6 years.

A key factor in both models is that they overestimate the column densities of almost every species considered. The simplest explanation for this is that our observed column densities are all lower limits based upon one or two detections of each species. The true column density may be higher than our derived lower limit and this would bring the model predictions better into line with the actual column densities. However some of the model column densities are factors of several hundred larger than the observed column densities and the true column density is unlikely to be several hundred times the observed lower limit. We have examined this in the case of the E-type form of methanol, for which we have sufficient transitions to form a rotation diagram. A lower limit to the methanol column density can be evaluated for each line used in the rotation diagram. The lower

limits when compared to the strict value determined from the rotation diagram do not differ by more than a factor of 2. On the evidence of E-type methanol the lower limits do not underestimate the true column density by a significant amount. This may not be true for all the molecules detected in our survey but we can be reasonably confident that the lower limits do not underestimate the true value by more than a factor of ten.

We also note that the column densities predicted by the model will be affected by departures from our assumptions about the molecular cloud (e.g. a spherical cloud at an assumed distance of 3.1 kpc). Column density is simply the number density of the species integrated through the depth of the cloud. If the cloud is not spherical to any great degree (as can be seen in Fig. 1 the HCO^+ emission traces a kidney-shaped cloud) the model cloud depth will not match the actual cloud depth and will give rise to errors in the predicted column density. The structural model on which the chemical model is based is that derived from the radiative transfer modelling of Heaton et al. (1993). The authors note the same problem and that the line profiles are reproduced excellently by assuming a spherical cloud.

Our model takes no account of optical depth, implicitly assuming that emission from all species is optically thin by integrating the column densities throughout the entire depth of the cloud. Optically thick emission arises predominantly from the surface layers of the cloud and column densities derived from optically thick lines will underestimate the actual column density throughout the whole cloud (i.e. the derived lower limits to column density in Table 2 are true lower limits even in the optically thick case). The lower limit to the column density of CO was obtained from the $C^{17}O$ 3–2 line, which is likely to be optically thin (the CO column density is obtained by assuming a $^{16}O/^{17}O$ ratio of 2400). CS is also likely to be optically thin or at most moderately optically thick as the isotopomer $C^{34}S$ is not detected (the maximum optical depth of CS is 2–3 if $C^{34}S$ is below the 5σ level). Other species may well possess some degree of optical depth and will in consequence have a larger actual column density than is observed. We note that CH_3OH observed towards hot core sources by Hatchell et al. (1998a) had optical depths of ~ 10, however these values are for observations towards the cores and not specifically towards the halo.

Given the above caveats we must reconcile the model predictions with the observations of the halo, in particular to estimate the degree of influence by the core. The model predicts that the column densities of methanol are strongly affected by the high column densities present toward the core (the core column density of methanol is some *4 orders of magnitude* greater than the halo, Millar et al. 1997). The observational evidence for this is somewhat limited. Methanol does not display an overly high rotation temperature (~ 30 K, as compared to the core temperature of ~ 300 K) as would be expected if the emission was predominantly from the core and the widths of the lines seen in the halo survey are roughly a third of those seen in the hot core survey of Paper I. This suggests that the methanol emission is more likely to originate from the halo rather than from dense hot gas picked up in the fringes of the beam. Other species, such as CS and HCN, have comparable linewidths in both core and halo and their halo emission might be due to pickup from the core. The beam-averaged model predicts no change in the column density of CS and a marginal change in the column density of HCN when the core is taken into account through beam-averaging. Further observations at larger angular distances from the core are necessary to confirm the core origins of HCN and CS.

The line widths and rotation temperature of the methanol suggest that the methanol emission is predominantly from the halo. This is at odds with the predictions of the beam-averaged model where the observed column densities of methanol are reproduced by the inclusion of warmer gas toward the core. The beam-averaged model does not however take into account the possibility of grain mantle evaporation in the halo. Temperatures in the inner regions of the halo may be high enough to evaporate volatile non-polar ices from grain mantles and enrich the gas-phase chemistry. If the temperature from the methanol rotation diagram is taken to be representative of the gas temperature, then the halo has an average temperature of ~ 30 K at this position. This compares to the predicted temperature from the structural model of 44 K at this position (0.3 pc from the core centre). The temperature of the innermost halo layers should be around 75 K, according to the structural model.

Large quantities of CO are present in grain mantle ices (Chiar et al. 1994, 1995). CO can react on the grain surface with hydrogen atoms, maintained by cosmic-ray processes, to produce CH_3OH (van Dishoeck & Blake 1998 and references therein). The constituents of the grain mantle ices evaporate at different temperatures, which may lead to a chemical stratification of the cloud. CO in non-polar ices is thought to evaporate at temperatures of 15–20 K, or if trapped in polar ices is expected to sublime at temperatures of ~ 60 K (Tielens et al. 1991). The temperature in the region of the halo sampled by the beam is certainly high enough to evaporate CO ice from grains, which may explain why the model does not reproduce the observed CO column densities.

Methanol has a higher sublimation temperature than CO; perhaps ~ 90 K if present in mixed polar ices (Sandford & Allamandola 1993). Methanol may sublime at lower temperatures than this if it is trapped in more volatile non-polar ices. However a greater understanding of the sublimation processes in molecular ice mantles is required to say whether this is plausible at the temperatures within the halo (~ 30 K). Alternatively the methanol in the halo may be the legacy of a higher temperature period in the halo, perhaps caused by shocks. The lack of core pickup predicted by the model must also be explained. If the column density of methanol is larger than expected in the halo, the core column density must be correspondingly reduced. In this case pickup of methanol from the core is much less important to the column density. Or more simply, the methanol core may be smaller than expected. Further observations of methanol in the halo at greater distances from the core are required to address these possibilities.

We have also investigated the model predictions of the column density of propyne (CH_3CCH) in the halo of G34.3. The observed propyne column density of 4.6×10^{14} cm^{-2} at an offset

(0, 20″) from the cloud centre (Hatchell et al. 1998a) was used. The model/observed ratios from both of our models at this position are $0.327 \rightarrow 5.85\times10^{-6}$ as the halo ages from $10^4 \rightarrow 10^6$ years in the single line of sight model and $0.459 \rightarrow 0.005$ as the halo ages from $10^4 \rightarrow 10^6$ years in the beam-averaged model. The beam-averaged model propyne column density is altered by core evolution, most notably in medium and old halo models (10^5 and 10^6 years) where the column density increases by an order of magnitude over 10^4 years. Neither the beam-averaged nor single line of sight model can reproduce the observed column density of propyne at late times. Propyne is likely to originate in the core, the linewidths seen in the halo are comparable to those in the core. The main production route of propyne in the model is via mantle-evaporated C_2H_4. However the high column density seen by Hatchell et al. (1998a) in the halo implies that the chemistry of propyne is not well understood.

The model overestimates the column densities of most species, particularly CS at all times of the model. One reason why the column density of CS in the model is much higher than observed may be that the initial abundance of sulphur is too high. In the compact and ultracompact cores sulphur is injected into the gas phase from grain mantles in the initial form of H_2S, with an abundance of 10^{-6}, following observations of the Orion Hot Core by Minh et al. (1990). A recent study of sulphur chemistry in hot cores (Hatchell et al. 1998b) shows that a lower initial abundance of H_2S (10^{-7}) may help to reproduce the observed column densities of CS. The column density of SO_2 also depends upon the intial sulphur abundance as both SO_2 and CS are mainly produced in the halo gas by reactions with atomic sulphur. A decrease of the initial abundance of atomic sulphur present in the halo corresponding to that of Hatchell et al. (1998b) would reduce model column densities by a factor of 10. A reduction in the elemental sulphur abundance in the halo by a factor of 10–50 would predict CS abundances much closer to those observed and alter the prediction of SO_2 for the halo age much more in line with other species, i.e. to an age of roughly 10^6 years.

Combining the predictions of all the species modelled leads to a rough timescale for the evolution of the halo, with a cautionary warning that the final results are sensitively dependent upon the initial abundances of the model (as seen above for the CS and SO_2 abundances). Different molecular tracers predict different ages for the halo and core (as can be seen in Tables 4 and 5). The consideration of the initial sulphur abundance and mantle-evaporation chemistry in the halo may remove the discrepancies between the different molecules, although further investigation is necessary to resolve their effects. If the initial sulphur abundance is too high then the halo is likely to be old (10^5–10^6 years), whereas if the evaporation of grain mantles is important for halo chemistry then the halo may be considerably younger. However when all of the molecules and their predicted column densities are considered the most likely age for the halo is 10^5–10^6 years. A young halo contains roughly two orders of magnitude more of HCN and CN than is observed. The column densities of certain molecules (CS and propyne) cannot be reproduced by either the beam-averaged or single line of sight models. The column density of methanol can be reproduced by the beam-averaged model but observational evidence (low rotational temperature and narrow linewidths) points to the methanol emission originating from the halo. We will discuss possible improvements to the radial chemical model in the next section.

7. Summary and conclusions

We have performed a 330–360 GHz molecular line survey of the halo gas surrounding the hot core associated with G34.26+0.15. The species detected are mainly simple diatomic or triatomic molecules, with the exceptions of formaldehyde and methanol. We have extended the chemical model of Paper II to predict the column densities of a general line of sight drawn through the model cloud and to predict beam-averaged column densities sampled by a gaussian beam. A comparison of single line of sight and beam-averaged models reveals that for most molecules the predicted column densities do not greatly differ between the two models, apart from a small increase in the column densities of the beam-averaged model. This is because the H_2 column density is slightly larger in the beam-averaged model than in the "pencil-beam" single line of sight model.

For certain molecules (CH_3OH and SO_2) the addition of beam-averaging has significant effects due to the influence of the core chemistry upon the beam-averaged column density. The observational evidence is against this; both SO_2 and CH_3OH have much narrower linewidths in the halo than in the core and a rotation diagram for CH_3OH yields a much lower temperature than that of the core, suggesting that the emission is mainly from the halo. Further observations with larger angular distances from the core and more detailed modelling of mantle evaporation processes are needed to confirm the origins of SO_2 and CH_3OH in the halo.

A comparison of our models with the observations shows that different species predict different ages for the cloud. The column densities of CO, C_2H, CN, H_2CO and HCN are reasonably consistent with a halo age of 10^6 years whereas the column densities of CH_3OH, SO_2 and HCO^+ are inconsistent with halo ages greater than 10^4 years. We have investigated the propyne (CH_3CCH) column density in the halo observed by Hatchell et al. (1998a) and find that neither model can reproduce the column density of propyne for halo ages of greater than 10^5 years. The high observed column densities of Hatchell et al. (1998a) suggest that propyne chemistry is poorly understood. Further observations and modelling are of the utmost importance in identifying the possible formation routes of CH_3CCH.

There are a number of approaches that may resolve the problems outlined above. The model does not take into account the evaporation of dust grain ice mantles in the inner layers of the halo, where the structural model and the CH_3OH rotation temperature predict that the temperature is high enough to evaporate CO. The addition of more detailed ice evaporation processes to the model will bring the predictions of the CO abundance better into line with that observed and may provide a better fit to the observed column densities of species such as CH_3OH

and H_2CO which are both thought to form on grain surfaces by hydrogen reactions with CO ice. As noted in Paper II and van Dishoeck & Blake (1998), the adoption of stratified grain mantle desorption within the cloud (i.e. grain mantle composition may vary radially through the cloud) leading to the concept of different species evaporating at different distances from the cloud centre could help to improve the radial chemical model of G34.26+0.15. Dust continuum observations are needed to provide information about the temperature of grain mantles in the halo of G34.26+0.15.

The initial abundance of sulphur in the chemical model may be too high by a factor of 10, as indicated by recent studies of hot core chemistry (Hatchell et al. 1998b). Reducing the value to that suggested reverses the prediction of SO_2 that the halo chemistry is young, instead lending weight to the supposition that the halo is older than 10^5 years. A reduction in the sulphur abundance would also bring the model predictions of CS better into line with those observed. We conclude that, based on current evidence, this is the most likely age for the halo given the agreement between CO, C_2H, H_2CO and HCN. However we note that if grain mantle evaporation is important in the inner layers of the halo then these timescales are likely to change as a substantial fraction of the CO and H_2CO in the halo may be directly evaporated from the grains rather than slowly built up by gas-phase chemistry.

An outstanding problem in the study of cold gas such as the halo of G34.26 is that many of the detected molecules are linear, implying that their transitions are spaced widely in frequency. The column densities of the species detected in the survey of the halo are thus almost all lower limits (with the exception of methanol). Multifrequency studies are needed to constrain the column densities of the observed linear species, perhaps by extending the survey into the 210–280 GHz range. Studies at many positions are needed to constrain the abundance profiles, these can be obtained efficiently (at least for low frequency lines) by using the new generation of array receivers in a similar manner to the surveys of the giant molecular clouds M17 and Cepheus A by Bergin et al. (1997). Optical depth effects not accounted for in our model can also be dealt with by coupling the chemical model with a radiative transfer model in a similar manner to that pursued in models of low mass star forming cores. A valuable first step in this direction has been achieved by Doty & Neufeld (1997) wherein the UMIST chemical model has been combined with the radiative transfer model of Doty (1997). However the number of species modelled is not large (they calculate line profiles of only CO and water isotopes) and there is scope for enhancing our knowledge of the cloud chemistry by matching the line profiles generated by model abundances to molecular line observations, using a less restrictive radiative transfer model such as that developed by Phillips & Little (1998).

Acknowledgements. MAT would like to thank PPARC for their support via a studentship and the JCMT staff for all their assistance during the observations. We would like to thank an anonymous referee for making several suggestions which substantially improved the content of this paper. Astrophysics research at the University of Kent and UMIST is supported via grants from PPARC.

References

Anderson T., Herbst E., Delucia F.C., 1993, J. Mol. Spectrosc. 159, 410
Andersson M., 1985, In: Shaver P.A., Kjar K. (eds.) ESO-IRAM-Onsala Workshop on (Sub)millimetre Astronomy. ESO, Garching, 353
Andersson M., Garay G., 1986, A&A 167, L1
Bergin E.A., Ungerechts H., Goldsmith P.F., et al., 1997, ApJ 482, 267
Carral P., Welch W.J., 1992, ApJ 385, 244
Caselli P., Hasegawa T.I., Herbst E., 1993, ApJ 405, 548
Cesaroni R., Churchwell E., Hofner P., Walmsley C.M., Kurtz S., 1994, A&A 288, 903
Charnley S.B, Millar T.J., 1994, MNRAS 270, 570
Charnley S.B., Tielens A.G.G.M., Millar T.J., 1992, ApJ 399, L71
Charnley S.B, Kress M.E., Tielens A.G.G.M., Millar T.J., 1995, ApJ 448, 232
Chiar J.E., Adamson A.J., Kerr T.H., Whittet D.C.B., 1994, ApJ 426, 240
Chiar J.E., Adamson A.J., Kerr T.H., Whittet D.C.B., 1995, ApJ 455, 234
Doty S.D., 1997, in preparation
Doty S.D., Neufeld D.A, 1997, ApJ 489, 122
Gaume R.A., Fey A.L., Claussen M.J., 1994, ApJ 432, 638
Hatchell J., Thompson M.A., Millar T.J., Macdonald G.H., 1998a, A&AS, in press
Hatchell J., Thompson M.A., Millar T.J., Macdonald G.H., 1998b, A&A, in press
Heaton B.D., Little L.T., Yamashita T., et al., 1993, A&A 278, 238
Heaton B.D., Matthews N., Little L.T., Dent W.R.F., 1985, MNRAS 217, 485
Heaton B.D., Little L.T., Bishop I.S, 1989, A&A 213, 148
Henkel C., Wilson T.L., Mauersberger R., 1987, A&A 182, 137
Jewell P.R., Hollis J.M., Lovas F.J., Snyder L.E., 1989, ApJS 70, 833
Kutner M.L., Ulich B.L., 1981, ApJ 250, 341
Lovas F.J., 1992, J. Phys. Chem. Ref. Data 21, 181
Macdonald G.H., Gibb A.G., Habing R.J., Millar T.J., 1996, A&AS 119, 333 (Paper I)
MacKay D.D.S, 1995, MNRAS 274, 694
Martin-Pintado J., Wilson T.L., Gardner F.F, Henkel C., 1985, A&A 142, 131
Matthews N., Little, L.T., Macdonald G.H., et al., 1987, ApJ 184, 284
Millar, T.J., Macdonald G.H., Gibb A.G., 1997, A&A 325, 1163 (Paper II)
Millar T.J, Herbst E., Charnley S.B., 1991, ApJ 369, 147
Olmi L., Cesaroni R., Neir R., Walmsley C.M., 1996, A&A 315, 565
Phillips R.R., Little L.T., 1998, in prep.
Poynter R.L., Pickett H.M., 1985, Appl Opt 24, 2335
Sandford S.A., Allamandola L.J., 1993, ApJ 417, 815
Serabyn E., Weisstein E.W, 1995, ApJ 451, 238
Tielens A.G.G.M, Tokunaga A.T., Geballe T.R., Baas F., 1991, ApJ 381, 181
Turner B.E., 1991, ApJS 76, 617
van Dishoeck E.F., Blake G.A., 1998, ARA&A, 36
Walmsley C.M., Schilke P, 1993, In: Millar T.J, Williams D.A (eds.) Dust and Chemistry in Astronomy. IoP Publishing, Bristol, p. 37
Wyrowski F., Walmsley C.M., 1996, A&A 314, 265